Nondegenerate four-wave mixing in rubidium vapor: The diamond configuration

F. E. Becerra,[1,2] R. T. Willis,[1] S. L. Rolston,[1] and L. A. Orozco[1]
[1]*Joint Quantum Institute, Department of Physics, University of Maryland and National Institute of Standards and Technology, College Park, Maryland 20742, USA*
[2]*Departamento de Física, CINVESTAV, Apdo. Post. 14-740, 07000 Mexico, Distrito Federal, Mexico*
(Received 16 April 2008; published 23 July 2008)

We investigate experimentally and theoretically nondegenerate four-wave mixing in rubidium vapor using a diamond configuration ($5S_{1/2}$, $5P_{1/2}$, $5P_{3/2}$, and $6S_{1/2}$ levels). We model this process of three classical fields interacting with a four-level atomic system with the Schrödinger equation. The experimental results are in good agreement with theoretical predictions for the generated light as a function of detuning.

DOI: 10.1103/PhysRevA.78.013834 PACS number(s): 42.65.Ky, 42.50.Gy, 32.80.Qk

I. INTRODUCTION

Four-wave mixing (FWM) is an effective way to generate correlations and entanglement in quantum optics. The simultaneous requirements of conservation of energy and momentum in the process facilitate the appearance of quantum coherences. FWM in an atomic vapor was the first method used to produce squeezed light [1]. The system is again the focus of intensive research through the connection with the Duan-Lukin-Cirac-Zoller protocol for the creation of entangled photons [2] and its realization in different atomic gases [3–5]. Recently, substantial twin-beam squeezing [6] has been observed using FWM in a double lambda configuration.

This paper presents our experimental and theoretical study of nondegenerate FWM in Rb vapor in a diamond configuration: a single ground state, two intermediate states, and an upper state. This system has been studied theoretically and experimentally in the past and has some unusual properties related to the phase sensitivity of the process and nonabsorptive states [7–11]. This configuration also allows the generation of light at telecommunication wavelengths using rubidium and cesium atoms [5,12], that can be applied to quantum information and quantum communication using atomic systems. Here we describe our investigations on the generation and characterization of light at telecommunication wavelength in a rubidium vapor cell via FWM.

II. EXPERIMENTAL SETUP

Figure 1 shows a four-level atomic system in a diamond configuration interacting with three waves of frequencies ω_i $(i=1,2,3)$. Level a is the ground state coupled to levels b and d by fields E_1 at frequency ω_1 and E_3 at frequency ω_3, respectively. Level c is coupled to level b by field E_2 at frequency ω_2 and to level d by the field resulting from the FWM process at frequency $\omega_4=\omega_1+\omega_2-\omega_3$ due to energy conservation. The atomic states in ^{87}Rb that we use to generate FWM light and map to the schematic of Fig. 1 are $|a\rangle=|5S_{1/2},F=2\rangle$, $|b\rangle=|5P_{1/2},F=1\rangle$, $|c\rangle=|6S_{1/2},F=2\rangle$, and $|d\rangle=|5P_{3/2},F=1\rangle$. The lifetimes of the exited levels are $\tau_b=27.8$ ns, $\tau_c=46$ ns, and $\tau_d=26.4$ ns.

Figure 2 shows a schematic of the experiment. Three beams in a nearly copropagating configuration overlap in the center of a heated rubidium cell. We heat the cell in an oven to 100 °C with a resistive wire producing a magnetic field about 0.5 G at the center of the cell along its axis. An InGaAs amplified photodetector with a long pass filter with a cutoff wavelength of 1350 nm collects the generated FWM light in the direction defined by phase matching. The 5-cm-long cell contains a natural mixture of ^{85}Rb and ^{87}Rb without buffer gas.

We study the FWM process in ^{87}Rb for different experimental configurations. Three beams from three lasers at wavelengths of 795, 780, and 1324 nm with diameters of 1 mm overlap in the vapor cell with relative angles that satisfy the phase matching condition, $\vec{k}_1+\vec{k}_2=\vec{k}_3+\vec{k}_4$. Figure 2 shows the angles among the three beams that generate FWM light at 1367 nm.

A titanium:sapphire laser with a linewidth of about 1 MHz, drives the $D1$ transition at 795 nm. This laser is locked to an atomic transition in an independent vapor cell, for example, the $5S_{1/2}$, $F=2$ to $5P_{1/2}$, $F'=1$ in ^{87}Rb from saturation spectroscopy. A 1324 nm diode laser with a linewidth <1 MHz drives the transition $5P_{1/2}\rightarrow 6S_{1/2}$. A temperature and current controlled laser diode (Sharp GH0781JA2C) at 780 nm drives the $D2$ transition. It has a Gaussian linewidth measured by self-homodyning (over 1/3 s) with a long delay fiber characterized by width (σ) of 11 MHz. The intensities of the beams at the center of the cell are typically around 15×10^4, 3×10^4, and 3×10^4 mW/cm^2, respectively. All the lasers are linearly polarized: the lasers at 795 and 1324 nm in the same direction, and the polarization of the generated light is the same as the 780 nm beam. The generation of FWM light decreases when the beams at 795 and 1324 nm

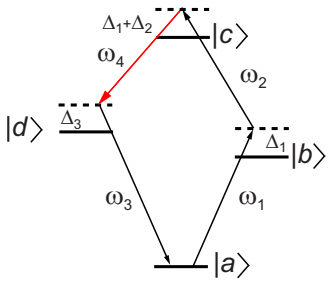

FIG. 1. (Color online) Four-level atom interacting with three external fields with frequencies ω_1, ω_2, and ω_3 and generated light via four-wave mixing at frequency ω_4.

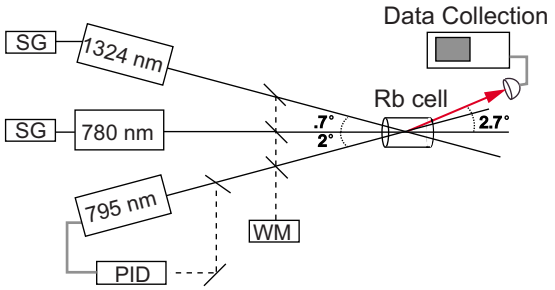

FIG. 2. (Color online) Experimental configuration. Three beams of different frequencies are overlapped in the heated rubidium cell. The generated FWM light at 1367 nm is collected and analyzed. SG are signal generators to scan the lasers; PID is a proportional, integral, and differential feedback control to lock the frequency of the 795 nm laser; WM is a wave meter. The angles satisfy phase matching.

have orthogonal polarizations. We record the output of the photodetector collecting the generated FWM light in a digital oscilloscope as we scan the frequency of the two diode lasers: the laser of 1324 nm at a rate of 0.1 Hz and the laser of 780 nm at a rate of 20 Hz. The experimental data consist of the intensity of the FWM generated light as a function of detunings of these two lasers from the specific atomic transitions for a given frequency of the 795 nm laser (see Fig. 3). We calibrate the frequency of the laser at 1324 nm with a wave meter of ± 30 MHz resolution. We use the absorption lines from a reference rubidium cell at room temperature to determine the frequency of the 780 nm laser during the data acquisition.

Figure 3 shows an example of experimental results for the generated light as a function of detunings of the 780 and 1324 nm lasers: (a) three-dimensional representation and (b) contour plot. The FWM generated light has a frequency $\omega_4 = \omega_{795} + \omega_{1324} - \omega_{780}$ due to energy conservation, and includes resonant features depending strongly on the detunings of the lasers. The features with labels in the contour plot [Fig. 3(b)] will be explained in Sec. IV.

III. THEORETICAL MODEL

We model this system as a four-level atom interacting with three different monochromatic external fields, each one coupling a single transition. Figure 1 shows this four-level atomic system in a diamond configuration interacting with three fields E_1, E_2, and E_3 of frequencies ω_i $(i=1,2,3)$, respectively, and generating FWM light at frequency ω_4. We solve the Schrödinger equation, ignoring decay, Doppler effect, and depletion of the pump beams; we obtain the atomic polarization of the system oscillating at ω_4, which describes the generated light from the FWM process. The Hamiltonian is

$$H = H_a + H'(t) = H_a - \vec{\mu} \cdot \vec{E}, \tag{1}$$

where H_a is the uncoupled atomic Hamiltonian and $H'(t)$ is the field-atom interaction Hamiltonian; $\vec{\mu}$ is the electric dipole moment and $\vec{E}$ is the total external field.

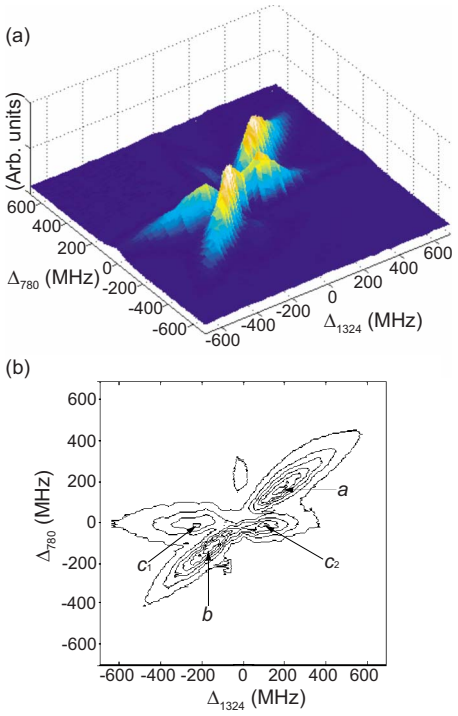

FIG. 3. (Color online) Generated light as a function of two different detunings for the laser at 795 nm on resonance for specific atomic transitions; (a) three-dimensional representation; (b) contour plot showing the different resonances. The atomic states in the diamond configuration of Fig. 1 are $|a\rangle = |5S_{1/2}, F=2\rangle$, $|b\rangle = |5P_{1/2}, F=1\rangle$, $|d\rangle = |5P_{3/2}, F=1\rangle$, and $|c\rangle = |6S_{1/2}, F=2\rangle$ in ^{87}Rb. False color image; large intensity white (white); low intensity blue (dark gray). See the text for an explanation of specific resonances labeled in the figure.

We write the total external field as a scalar (our model does not take into account any polarization effects) as follows:

$$E(t) = \sum_{j=1}^{3} E_j \exp(-i\omega_j t) + \text{c.c.}, \tag{2}$$

where E_j are the amplitudes of the fields in the process, and we have ignored the spatial dependence of the field, and any propagation effects.

The wave function $|\Psi\rangle$ describes the state of the system, which we write in terms of the eigenstates of the free atomic system as

$$|\Psi\rangle = \sum_{k=a,b,c,d} C_k(t) \exp(-i\omega_k t) |k\rangle, \tag{3}$$

where $\omega_{a,b,c,d}$ are the atomic energies and $H_a|k\rangle = \hbar\omega_k|k\rangle$. The coefficients $C_k(t)$ are the probability amplitudes that the system is in the state $|k\rangle$ and describe the evolution of the state. In the rotating wave approximation, the amplitudes evolve due to H' as

$$\frac{d}{dt}\begin{pmatrix} C_a(t) \\ C_b(t) \\ C_c(t) \\ C_d(t) \end{pmatrix} = i\begin{pmatrix} 0 & \Omega_1^* e^{i\Delta_1 t} & 0 & \Omega_3^* e^{i\Delta_3 t} \\ \Omega_1 e^{-i\Delta_1 t} & 0 & \Omega_2^* e^{i\Delta_2 t} & 0 \\ 0 & \Omega_2 e^{-i\Delta_2 t} & 0 & 0 \\ \Omega_3 e^{-i\Delta_3 t} & 0 & 0 & 0 \end{pmatrix} \times \begin{pmatrix} C_a(t) \\ C_b(t) \\ C_c(t) \\ C_d(t) \end{pmatrix}, \tag{4}$$

where $\Delta_j = \omega_j - \omega_{nm}$ are the detunings of the fields from the corresponding transitions $\omega_{nm} = \omega_n - \omega_m$, $(m,n = a,b,c,d)$ given by

$$\Delta_1 = \omega_1 - \omega_{ba}, \quad \Delta_2 = \omega_2 - \omega_{cb}, \quad \Delta_3 = \omega_3 - \omega_{da}, \tag{5}$$

and $\Omega_j = \vec{E}_j \cdot \vec{\mu}/\hbar$ are the atomic Rabi frequencies.

We solve Eq. (4) assuming a trial solution for level d of the form $C_d(t) = Ae^{i\beta t}$, where β is time independent. We use this expression in Eq. (4) to find the coefficients C_b, C_c, and C_a in terms of the coefficients A, and the characteristic energies β [13] (quasienergies). The coefficients $C_k(t)$ are

$$C_a(t) = \frac{1}{\Omega_3}\sum_{j=1}^{4} \beta_j A_j e^{i(\beta_j + \Delta_3)t},$$

$$C_b(t) = \frac{1}{\Omega_3 \Omega_1^*}\sum_{j=1}^{4} \alpha_j A_j e^{i(\beta_j + \Delta_3 - \Delta_1)t},$$

$$C_c(t) = \frac{\Omega_2}{\Omega_3 \Omega_1^*}\sum_{j=1}^{4} \frac{\alpha_j}{\kappa_j} A_j e^{i\kappa_j t},$$

$$C_d(t) = \sum_{j=1}^{4} A_j e^{i\beta_j t}, \tag{6}$$

where $\alpha_j = \beta_j(\beta_j + \Delta_3) - \Omega_3^2$ and $\kappa_j = \beta_j + \Delta_3 - (\Delta_1 + \Delta_2) = \beta_j - \Delta_4$, for the quasienergies defined as the four roots of the equation

$$[\kappa(\kappa + \Delta_2) - \Omega_2^2][\beta(\beta + \Delta_3) - \Omega_3^2] = \kappa\beta\Omega_1^2. \tag{7}$$

We can find the analytical expressions for these coefficients by assuming that all the population is in the ground state $|a\rangle$ at $t=0$, so that $C_a(0)=1$ and $C_b(0)=C_c(0)=C_d(0)=0$. Applying this initial condition to Eqs. (6), we obtain a time-independent algebraic equation for the coefficients A_j in terms of detunings, Rabi frequencies, and the quasienergies β_j as follows:

$$A_1 = F\frac{\kappa_1\{-(\beta_3+\Delta_3)(\beta_4+\Delta_3)\Delta_4 + (\beta_3+\beta_4+\Delta_3-\Delta_4)\Omega_3^2 + \beta_2[\beta_3\beta_4 - (\beta_3+\beta_4+\Delta_3)\Delta_4 + \Omega_3^2]\}}{(\beta_1-\beta_2)(\beta_1-\beta_3)(\beta_1-\beta_4)},$$

$$A_2 = F\frac{\kappa_2\{(\beta_3+\Delta_3)(\beta_4+\Delta_3)\Delta_4 - (\beta_3+\beta_4+\Delta_3-\Delta_4)\Omega_3^2 + \beta_1[-\beta_3\beta_4 + (\beta_3+\beta_4+\Delta_3)\Delta_4 - \Omega_3^2]\}}{(\beta_1-\beta_2)(\beta_2-\beta_3)(\beta_2-\beta_4)},$$

$$A_3 = F\frac{\kappa_3\{-(\beta_2+\Delta_3)(\beta_4+\Delta_3)\Delta_4 + (\beta_2+\beta_4+\Delta_3-\Delta_4)\Omega_3^2 + \beta_1[\beta_2\beta_4 - (\beta_2+\beta_4+\Delta_3)\Delta_4 - \Omega_3^2]\}}{(\beta_1-\beta_3)(\beta_2-\beta_3)(\beta_3-\beta_4)},$$

$$A_4 = F\frac{\kappa_4\{(\beta_2+\Delta_3)(\beta_3+\Delta_3)\Delta_4 - (\beta_2+\beta_3+\Delta_3-\Delta_4)\Omega_3^2 + \beta_1[-\beta_2\beta_3 + (\beta_2+\beta_3+\Delta_3)\Delta_4 - \Omega_3^2]\}}{(\beta_1-\beta_4)(-\beta_2+\beta_4)(-\beta_3+\beta_4)}, \tag{8}$$

where the factor

$$F = \Omega_3/[(\Delta_1+\Delta_2)(\Delta_1+\Delta_2-\Delta_3) - \Omega_3^2] \tag{9}$$

is a common factor contributing to the location of the resonances. Each coefficient $C_j(t)$ oscillates at four different frequencies related to the solutions of Eq. (7) β_i $(i=1,2,3,4)$. Figure 4 shows the quasienergies, at given Rabi frequencies, for a fixed Δ_3 detuning and for two different Δ_1 detunings as a function of the detuning Δ_2 (solid lines). The dashed lines correspond to the uncoupled atomic system. The choice of parameters in the plot is compatible with our experimental realization. Note the avoided crossings in the quasienergies of the field-atom coupled system for different Δ_1 detunings.

The amplitude of the generated light from the FWM process at frequency ω_4 is proportional to the component of the atomic polarization oscillating at the same frequency. Components oscillating at other frequencies do not satisfy energy conservation and do not contribute to the process.

The atomic polarization related to the transition $|c\rangle \rightarrow |d\rangle$ contains only four terms oscillating at the frequency ω_4 and 12 oscillating at different frequencies as follows:

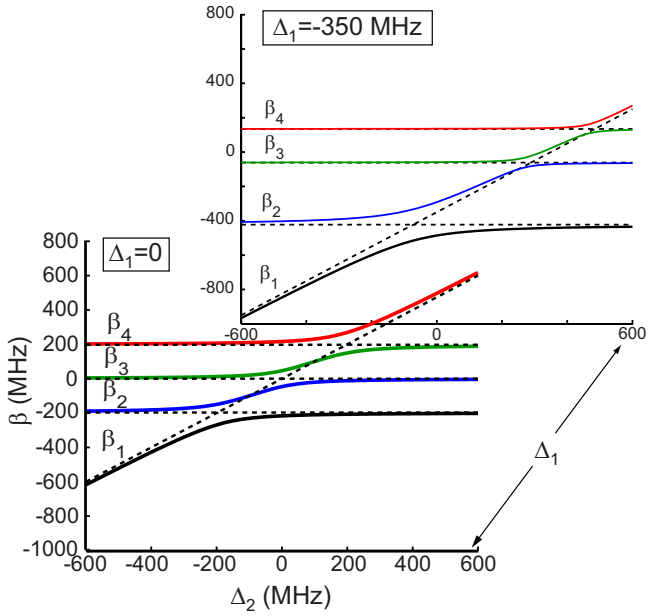

FIG. 4. (Color online) Quasienergies for coupled (solid lines) and uncoupled (dashed lines) atomic systems. The quasienergy β_i, root of Eq. (7), is related to the coefficient A_i. The parameters for the plot are $(\Omega_1,\Omega_2,\Omega_3,\Delta_3)/2\pi=(170,100,100,0)$ MHz for two different Δ_1 detunings: $\Delta_1=0$ (front plane) and $\Delta_1/2\pi=-350$ MHz (back plane).

$$P_{cd} = \mu_{cd} C_c^*(t) C_d(t) e^{-i\omega_{cd}t} + \text{c.c.}$$
$$= \sum_{j=1}^{4} P_{cd}^{j} e^{-i\omega_4 t} + \sum_{j,k=1, j\neq k}^{4} P_{cd}^{kj} e^{-i(\omega_4+\beta_{jk})t}, \qquad (10)$$

where $\beta_{jk}=\beta_j-\beta_k\neq 0$ for $k\neq j$, and P_{cd}^{j} is the term of the atomic polarization oscillating at the frequency ω_4 describing the transition $|c,\beta_j\rangle\rightarrow|d,\beta_j\rangle$ associated to the same quasienergy β_j. The four terms describing the generation of light via FWM under these assumptions are

$$P_{cd}(\omega_4) = \sum_{j=1}^{4} P_{cd}^{j}(\beta_j) = \mu_{cd} \sum_{j=1}^{4} \frac{\alpha_j}{\kappa_j} A_j^2. \qquad (11)$$

The generation of FWM light has four contributions from four different terms, each one resonant near the avoided crossings of its related quasienergy in the atom-field coupled system [see Eq. (8)], characteristic in some multilevel atoms [14,15]. The term F in Eq. (9) is a global resonance contributing to the location of the generated light as a function of detunings. This factor enhances the generation of light for specific detunings independent of the quasienergies.

IV. ANALYSIS

The generated light, as seen in Fig. 3, includes resonant features that depend strongly on the detunings of the 1324 and 780 nm lasers for a given 795 nm laser frequency. The light at the diagonal resonances in Fig. 3(b) (a,b), assuming energy conservation, has frequency $\omega_4\simeq\omega_{cd}$ (frequency of the atomic transition from $5P_{3/2}$ to $6S_{1/2}$ in Rb), because

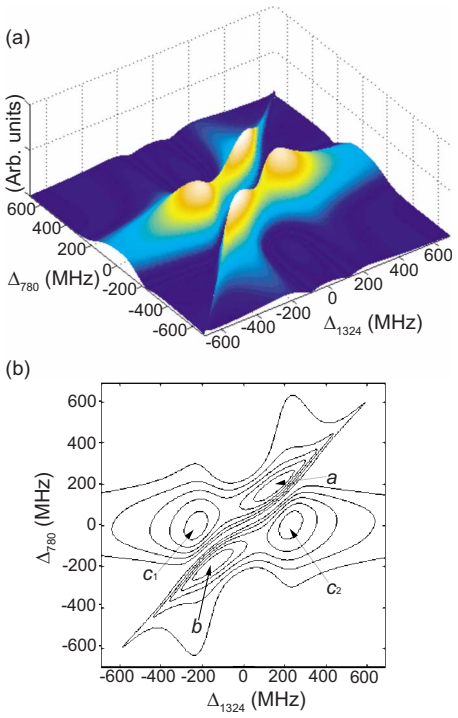

FIG. 5. (Color online) Theoretical atomic polarization oscillating at ω_4 calculated in Eq. (11) for $(\Omega_1,\Omega_2,\Omega_3)/2\pi=(170,100,100)$ MHz and $\Delta_1=0$; (a) three-dimensional representation; (b) contour plot. These conditions are similar to the experimental values of Fig. 3.

these resonances appear at $\Delta_{1324}\simeq\Delta_{780}$, and then the detuning of the FWM light from the respective atomic transition is $\Delta_4=\Delta_{1324}-\Delta_{780}\simeq 0$. The other two resonances in Fig. 3(b) (c_1,c_2) appear when the 780 nm laser is on resonance, $\Delta_{780}\simeq 0$, and then the generated light has a frequency $\omega_4\simeq\omega_{cd}+\Delta_{1324}$.

The expected generated light in the FWM process is proportional to the absolute value of the atomic polarization, $|P_{cd}(\omega_4)|$, described in Eq. (11). Figure 5 shows the three-dimensional representation (a) and the contour plot (b) of the calculated atomic polarization oscillating at frequency ω_4 from Eq. (11) in units of dipole moment μ_{cd} for the Rabi frequencies $(\Omega_{795},\Omega_{780},\Omega_{1324})/2\pi=(170,100,100)$ MHz, chosen so that the generated light qualitatively matches the data. We estimate the experimental atomic Rabi frequencies from the intensities of the beams at the center of the cell and the dipole moments in Refs. [12,16,17] as $(\Omega_{795},\Omega_{780},\Omega_{1324})/2\pi=(385,170,120)$ MHz; we assumed no light scattering, and we corrected for losses from the windows. Because of the absorption in the cell of the 795 nm light on resonance, and the 780 nm close to resonance in a Doppler broadened medium, we expect smaller Rabi frequencies than the ones we calculated to enter in the process. However, the Rabi frequencies used in the calculated atomic response should be of the order of the experimental Rabi frequencies.

Figure 6 shows the absolute value of the four terms of the atomic polarization associated with the quasienergies of the system, in units of dipole moment μ_{cd}, with the 795 nm laser on resonance. Every term $|P_{cd}^{i}|$ shows different resonances

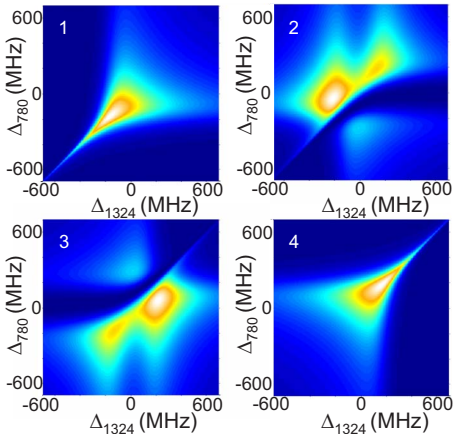

FIG. 6. (Color online) Absolute value of the four contributions to the atomic response calculated with Eq. (11) as a function of detunings for the laser at 795 nm on resonance. Figure 5(a) shows the total atomic response where single contributions add together in the generation of FWM light.

near the avoided crossings of its respective quasienergy β_i, and is modulated by factors in the denominators of the coefficients A_i in Eq. (8).

The term $P^i_{cd}(\beta_i)=\alpha_i/\kappa_i A_i^2$ in the atomic response in Eq. (11) is resonant at the avoided crossings of its quasienergy β_i with the other quasienergies: $(\beta_i-\beta_j)\to 0$ for $j\neq i$. Quasienergies with single avoided crossings produce single resonances, while quasienergies with double avoided crossings produce double resonances. Since the location of the avoided crossings depends on the detunings, the resonances displace for different detunings. The terms $P^1_{cd}(\beta_1)$ and $P^4_{cd}(\beta_4)$ are resonant at $(\beta_1-\beta_2)\to 0$ and $(\beta_4-\beta_3)\to 0$, due to the single avoided crossings of β_1 and β_4, respectively (see Fig. 4). Figures 6(1) and 6(4) show single resonant terms $|P^1_{cd}(\beta_1)|$ and $|P^4_{cd}(\beta_4)|$ related to β_1 and β_4, respectively. The terms $P^2_{cd}(\beta_2)$ and $P^3_{cd}(\beta_3)$ are resonant at $(\beta_2-\beta_1(3))\to 0$ and $(\beta_3-\beta_2(4))\to 0$, respectively, due to the double avoided crossings of β_2 and β_3 (See Fig. 4). Figures 6(2) and 6(3) show the double resonant terms $|P^2_{cd}(\beta_2)|$ and $|P^3_{cd}(\beta_3)|$ related to β_2 and β_3, respectively. Note that the extra resonances for these last terms come from one of the avoided crossings that is relocated for different Δ_3 detunings, as shown in Fig. 4 in the case of different Δ_1 detunings.

The generated light is the result of the four contributions to the atomic polarization containing single and double resonances adding together to form the resonant structure shown in Fig. 3 (experiment) and Fig. 5 (theory). Figure 7 shows the experimentally measured location of the FWM resonance as a function of detunings when the laser at 795 nm is detuned from the atomic resonance. The structure of the generated light in this case is a diagonal in the $(\Delta_{1324},\Delta_{780})$ plane. The diagonal resonance a (b) in Fig. 3 is more resonant when we red (blue) detune the 795 nm laser.

The common factor F in Eq. (9) displaces the avoided crossings of the quasienergies; positive detunings in Δ_{795} shift some avoided crossings to negative detunings in Δ_{1324} roughly the same amount, and vice versa. Figure 4 shows the avoided crossings for $\Delta_{795}=0$ and $\Delta_{795}/2\pi=-350$ MHz. The terms of the atomic polarization related to quasienergies

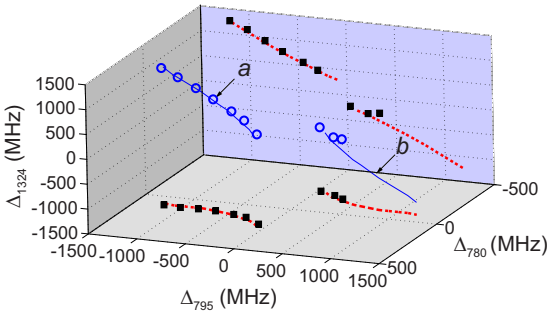

FIG. 7. (Color online) Location of the FWM resonance as a function of the three laser detunings corresponding to the resonances a and b in Fig. 3 for negative and positive 795 detuning, respectively. The ^{87}Rb atomic states involved in this measurement are $|a\rangle=|5S_{1/2},F=2\rangle$, $|b\rangle=|5P_{1/2},F=1\rangle$, $|d\rangle=|5P_{3/2},F=1\rangle$, and $|c\rangle=|6S_{1/2},F=2\rangle$ in a diamond configuration (see Fig. 1). Open circles are experimental results and blue (solid) lines are our theoretical predictions. The red (dashed) lines are the projections on the planes $\Delta_{1324}=-1500$ MHz and $\Delta_{780}=-500$ MHz.

with shifted avoided crossings produce the FWM light for $\Delta_{795}\neq 0$.

We detune the 795 nm laser below resonance (negative detuning), and we observe good agreement of the experimental result with the theoretical predictions (see Fig. 7). When we detune the laser above resonance (positive detunings) we do not observe generated FWM light after a detuning of 300 MHz. The presence of strong absorption of the 795 nm light by the level $5S_{1/2},F=2$ prevents further generation from the 87 isotope.

Figure 8 shows the two photon and 780 detunings of the FWM resonance measured as a function of detuning Δ_{795}. The location in frequency of the FWM resonance is such that the two photon detuning $\Delta_{2\ photon}=\Delta_{795}+\Delta_{1324}$ remains between 200 and 50 MHz, while the detuning Δ_{780} is on the same order. The error bars come from the precision of the wave meter. These detunings cancel each other in the detuning of the generated light so that $\Delta_4=\Delta_{2\ photon}-\Delta_{780}\sim 0$. As a result, the generated FWM light for the laser at 795 nm off resonance has the same frequency of the atomic transition $\omega_4\sim\omega_{cd}$.

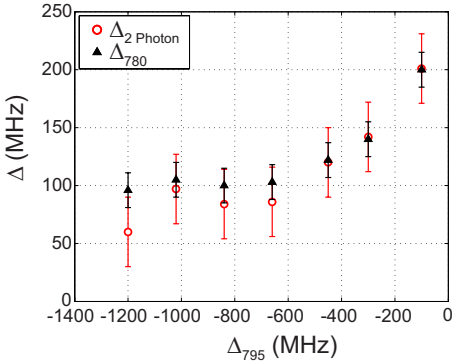

FIG. 8. (Color online) Two photon and 780 detunings of the location of the FWM resonance as a function of Δ_{795}. The resulting detuning for the generated light by FWM from the atomic transition is $\Delta_4\sim 0$.

V. CONCLUSION

We have studied experimentally and theoretically nondegenerate FWM in rubidium vapor using a diamond configuration ($5S_{1/2}$, $5P_{1/2}$, $5P_{3/2}$, and $6S_{1/2}$ levels). We studied the generated light as a function of the involved detunings and Rabi frequencies. The FWM process is resonant in the avoided crossings of the quasienergies of the system, which depend on the strength of the interaction and the detunings of the lasers from specific atomic transitions. There are four terms contributing to the atomic response that are related to the quasienergies. Every term is resonant at the location of the avoided crossings of its related quasienergy as a function of detunings. A common factor in the atomic response, independent of the quasienergies, shifts the avoided crossings in frequencies, displacing the FWM resonances for different detunings. The FWM light as a function of three different detunings comes from the terms in the atomic response with shifted avoided crossings. These displacements of the FWM resonance conserve a zero detuning of the FWM light; the generated light in this regime has the same frequency of the related atomic transition.

ACKNOWLEDGMENTS

This work was supported by NSF, DURIP, and CONACYT. We thank K. R. Sreenivasan for his interest and support of F.E.B. to pursue this project.

[1] R. E. Slusher, L. W. Hollberg, B. Yurke, J. C. Mertz, and J. F. Valley, Phys. Rev. Lett. **55**, 2409 (1985).
[2] L.-M. Duan, M. D. Lukin, J. I. Cirac, and P. Zoller, Nature (London) **414**, 413 (2001).
[3] A. Kuzmich, W. P. Bowen, A. D. Booze, A. Boca, C. W. Chou, L.-M. Duan, and H. J. Kimble, Nature (London) **423**, 731 (2003).
[4] C. H. van der Wal, M. D. Eisaman, A. André, R. L. Walsworth, D. F. Phillips, A. S. Zibrov, and M. D. Lukin, Science **301**, 196 (2003).
[5] T. Chanelière, D. N. Matsukevich, S. D. Jenkins, T. A. B. Kennedy, M. S. Chapman, and A. Kuzmich, Phys. Rev. Lett. **96**, 093604 (2006).
[6] C. F. McCormick, V. Boyer, E. Arimondo, and P. D. Lett, Opt. Lett. **32**, 178 (2007).
[7] M. C. Stowe, A. Pe'er, and J. Ye, Phys. Rev. Lett. **100**, 203001 (2008).
[8] S. Kajari-Schröder, G. Morigi, S. Franke-Arnold, and G.-L. Oppo, Phys. Rev. A **75**, 013816 (2007).
[9] D. A. Shapiro, JETP **88**, 1072 (1999).
[10] M. D. Lukin, S. F. Yelin, M. Fleischhauer, and M. O. Scully, Phys. Rev. A **60**, 3225 (1999).
[11] P. S. Hsu, A. K. Patnaik, and G. R. Welch, Opt. Lett. **33**, 381 (2008).
[12] E. Gomez, F. Baumer, A. D. Lange, G. D. Sprouse, and L. A. Orozco, Phys. Rev. A **72**, 012502 (2005).
[13] B. Kryzhanovsky and B. Glushko, Phys. Rev. A **46**, 2831 (1992).
[14] M. P. Sharma and J. A. Roversi, Phys. Rev. A **29**, 3264 (1984).
[15] S. N. Sandhya, Phys. Rev. A **75**, 013809 (2007).
[16] J. E. Simsarian, L. A. Orozco, G. D. Sprouse, and W. Z. Zhao, Phys. Rev. A **57**, 2448 (1998).
[17] M. S. Safronova, W. R. Johnson, and A. Derevianko, Phys. Rev. A **60**, 4476 (1999).